Dynamic properties of liquid alkaline-earth metals

M. M. G. Alemany,[1] J. Casas,[2] C. Rey,[1] L. E. González,[2] and L. J. Gallego[1]
[1]*Departamento de Física de la Materia Condensada, Facultad de Física, Universidad de Santiago de Compostela, E-15706 Santiago de Compostela, Spain*
[2]*Departamento de Física Teórica, Facultad de Ciencias, Universidad de Valladolid, E-47011 Valladolid, Spain*
(Received 30 July 1997)

Molecular dynamics simulations and theoretical calculations are used to study the static structure and dynamic properties of the liquid alkaline earths near their melting points. Where possible, comparison with experiments lends support to the reliability of the potentials used. On the other hand, comparison between theory and simulation enables a discussion of the limitations of the theory and its possible improvements. [S1063-651X(97)12812-4]

PACS number(s): 61.20.Gy, 61.20.Lc, 61.25.Mv, 61.20.Ja

I. INTRODUCTION

During the last decade the study of the dynamic properties of liquid metals has been the subject of numerous investigations, both experimental and theoretical (see, e.g., Ref. [1] for an overview). The liquid alkali metals have been in particular the most thoroughly studied ones. Inelastic neutron scattering has been used for the investigation of almost all the alkalis [2–5]. Molecular dynamics (MD) simulations, when provided with suitable realistic interionic potentials, are also an extremely useful tool for the investigation of liquids at a microscopic level, since they provide detailed information of the atomic trajectories which complements the partial information that can be extracted from experiments, and also gives access to some dynamic properties which are very difficult (in some cases impossible) to obtain experimentally. The key ingredient of MD simulations, i.e., realistic interionic potentials, are readily available for the alkali metals, such as those derived from the empty core model pseudopotential [6], or those derived from first principles, like the neutral pseudoatom (NPA) pseudopotential [7,8]. Based on this availability, dynamic (as well as static) properties of the liquid alkali metals have also been studied by MD simulations [9–14].

Compared with the alkali metals, their neighbors in the periodic table, i.e., the liquid alkaline earths, have received much less attention. Experimental measurements of their static structure [15] have been reported and also some thermodynamic and transport properties [16,17] have been measured. On the other hand, at least to our knowledge, no experimental investigation of their dynamic properties has been performed. With respect to MD simulations, we are only aware of a study of liquid alkaline earths using optimized plane wave pseudopotentials [18] that focused only on the static structure. This scarceness of simulations is probably due to the corresponding scarceness of reliable potentials. Recently, Gonzalez *et al.* [19] proposed effective interionic potentials obtained from the NPA method which, when used together with an accurate liquid state theory, produce static structure factors in good agreement with the experimental ones. A first aim in this work is to reassure the reliability of these potentials by obtaining ''exact'' MD structure factors to compare them with experiment, and also to obtain a first description of the dynamic behavior of the alkaline-earth liquid metals near their melting points.

Besides experimental and MD studies of the dynamics of liquids, theoretical investigation has also made a considerable progress in the last few years due to the development of nonphenomenological approaches based on the recognition of the appearance of two different dynamic processes in the evolution of time-dependent properties [20]. The first one, which gives rise to a rapid initial decay, is due to fast uncorrelated short-range interactions, which can be broadly identified with ''binary'' collisions. The second process, which usually leads to a long-time tail, is attributed to couplings of the dynamic variable of interest with other slowly decaying collective variables (called ''modes''), and therefore it is referred to as a mode-coupling process. Although the expressions involved in the evaluation of these two contributions to the dynamic properties are rather complicated, in some cases it is possible to make some simplifying approximations leading to more tractable expressions, while retaining the essential physical features of the processes. Within this line, Balucani and co-workers [10,21,22] made a thorough theoretical study of the dynamic properties of liquid alkali metals using potentials derived from the empty core model. More recently, a scheme has been developed [23] that enables a fully consistent determination of all the single-particle dynamic properties (velocity autocorrelation function, mean square displacement, self-intermediate scattering function, and diffusion coefficient). This scheme was applied to study the dynamic properties of liquid Li close to its melting point, leading to rather good results as compared to MD and experimental data. A second aim in this work is to check the reliability of this theory by comparing with MD simulations, and to assess the degree of applicability of the approximations involved in the theory as well as the possible improvements that can be made.

In Sec. II we briefly comment on the interionic potentials used in this work, and in Secs. III and IV we describe the MD simulations and the theory applied. In Sec. V we discuss the results obtained, and, finally, in Sec. VI, a summary of conclusions is given.

II. EFFECTIVE INTERIONIC PAIR POTENTIALS

The interionic pair potentials used in this work for the calculation of the dynamic properties of the liquid alkaline-

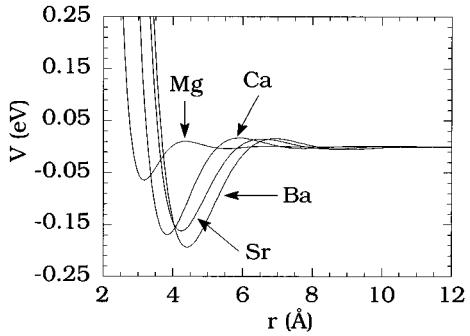

FIG. 1. Effective interionic pair potentials used in this work.

earth metals are the same as those of Ref. [19]. They are obtained using the NPA method, which is very briefly described next; for more details, see Ref. [19] and references cited therein.

The construction of effective interionic pair potentials for simple metals is based on the use of pseudopotentials to describe the ion-electron interaction, and the application of second-order perturbation theory of a uniform electron gas — linear response theory (LRT) — in order to calculate the energy of the system. The resulting expression gives the effective pair potential as a sum of the direct Coulomb repulsion between the ions and an electron-mediated part which is obtained in terms of the pseudopotential and the response function of the uniform electron gas. The exchange and correlation effects are introduced in the response function as a local field factor via the local density approximation.

The NPA pseudopotential is constructed as follows. First, the electron density displaced by an ion embedded in the electron gas is obtained from first principles using density functional theory. Second, the density is smoothed so as to eliminate the core-orthogonality oscillations that cannot appear with a pseudopotential. Finally, a local pseudopotential is constructed such that, when used within LRT, it reproduces the same smoothed electron density. The pair potentials thus obtained for the liquid alkaline-earth metals close to their melting points are shown in Fig. 1. The densities and temperatures of the systems are given in Table I. It must be stressed that the pair potentials are density dependent, and this fact implies that not all the thermodynamic properties can be meaningfully obtained in computer simulations.

III. MOLECULAR DYNAMICS SIMULATIONS

Using the potentials described in Sec. II, we simulated liquid Mg, Ca, Sr, and Ba at the states shown in Table I. In all cases, the simulations were performed by considering a system of $N=864$ atoms in a cubic box with periodic boundary conditions. The potentials were truncated at radii r_c (see Table I), which in each case was taken to correspond with the position of the maximum or minimum of the potential just before the largest distance allowed by the periodic boundary conditions, one-half the boxlength. At the cutoff radii, the potentials for Mg, Ca, Sr, and Ba have respectively dropped to 0.15%, 0.06%, 0.10%, and 0.11% of the values at the first attractive minima.

TABLE I. Thermodynamic states considered in this work and cutoff radii used in the MD simulations.

	ρ (Å^{-3})	T (K)	r_c (Å)
Mg	0.038 29	953	14.100
Ca	0.020 58	1123	17.225
Sr	0.016 36	1053	18.711
Ba	0.014 56	1003	18.768

The computational procedure was as follows. For each system, at the chosen density and temperature, a canonical MD simulation was first carried out using the Nosé constant temperature method [24]. The initial configuration was obtained from melting a fcc structure. The equations of motion were solved using a fourth-order Gear predictor-corrector algorithm [25] with a time step Δt of 0.002 ps. The energy of the system was then calculated by averaging over 2×10^4 time steps.

Starting now from a configuration with an energy close to the average value obtained as indicated above, microcanonical MD simulations were performed using the velocity Verlet algorithm [25] with the same time step as above, $\Delta t=0.002$ ps (microcanonical simulations are better than canonical simulations for studying dynamic properties because of the difficulty in controlling the heat exchange rate variable in the Nosé method). For Mg, this guarantees conservation of the total energy to within 0.004%; for the other metals, the conservation of the energy is even better. The positions $\mathbf{r}_i$ and velocities $\mathbf{v}_i$ of the particles were recorded every five time steps. The properties of interest were obtained by averaging over 2×10^5 time steps after an initial equilibration period of 25×10^3 time steps. Although standard, we give below, for completeness, the expressions used to compute the thermodynamic, structural, and time-dependent properties analyzed in this work (for more details about the theoretical background, we refer the reader to Refs. [25–29]); technical details are also given when strictly necessary.

In our simulations we obtained the specific heat at a constant volume; the distribution functions that describe the static structure of the systems, namely, the pair distribution function $g(r)$ and the structure factor $S(q)$; some time correlation functions, namely, the mean square displacement $\langle\Delta r^2(t)\rangle$ and the normalized velocity autocorrelation function $Z(t)$, which are related to the diffusion coefficient D; and the stress autocorrelation function $\eta(t)$, which is related to the shear viscosity η_s.

The isometric specific heat (per atom) was obtained using the expression

$$C_v=\frac{k}{N}\left[1-\left(1-\frac{2}{3N-3}\right)\langle E_{\rm kin}\rangle\langle E_{\rm kin}^{-1}\rangle\right]^{-1}, \qquad (1)$$

where k is the Boltzmann constant, $E_{\rm kin}$ is the total kinetic energy, and the angular brackets denote an average over an entire run.

The pair distribution function $g(r)$ was obtained by averaging the number of pairs of particles separated by a distance between r and $r+\delta r$ [25], whereas the static structure factor was computed as

$$S(q)=\frac{1}{N}\left\langle\sum_{i=1}^{N}\sum_{j=1}^{N}\exp[-i\mathbf{q}\cdot(\mathbf{r}_i-\mathbf{r}_j)]\right\rangle, \qquad (2)$$

q being a wave vector compatible with the periodic boundary conditions, i.e., $\mathbf{q}=(2\pi/L)(n_x,n_y,n_z)$, where L is the length of the simulation box and n_α are integers. The angular brackets in Eq. (2) denote averaging both over the trajectories of the particles [10^4 recorded configurations, each one separated by 10 Δt, were considered for computing $S(q)$] and over all the N_q directions corresponding to the same modulus q.

Two different time-dependent correlation functions related to the diffusion coefficient were computed. One is the mean square displacement

$$\langle \Delta r^2(t)\rangle = \frac{1}{N}\left\langle \sum_{i=1}^{N} [\mathbf{r}_i(t)-\mathbf{r}_i(0)]^2 \right\rangle, \tag{3}$$

from which D is obtained using the Einstein relation

$$D=\lim_{t\to\infty}\frac{\langle \Delta r^2(t)\rangle}{6t}. \tag{4}$$

The other is the normalized velocity autocorrelation function $Z(t)$, defined as

$$Z(t)=\frac{\left\langle \sum_{i=1}^{N} \mathbf{v}_i(t)\cdot\mathbf{v}_i(0) \right\rangle}{\left\langle \sum_{i=1}^{N} v_i(0)^2 \right\rangle}, \tag{5}$$

which allows one to obtain the self-diffusion constant through the Green-Kubo formula

$$D=\frac{kT}{m}\int_0^\infty dt\ Z(t), \tag{6}$$

where m is the atomic mass. Both methods for calculating D gave consistent results for all the metals studied in this paper. The dynamic correlation functions given by Eqs. (3) and (5) were computed by averaging over 7680 time origins, each one separated by 25 Δt. These two functions are in fact related to each other by the equation

$$\langle \Delta r^2(t)\rangle = \frac{6kT}{m}\int_0^t d\tau (t-\tau) Z(\tau). \tag{7}$$

A central magnitude in our study is the memory function of the velocity autocorrelation function, $K(t)$, which is defined by the Volterra equation

$$\dot{Z}(t)=-\int_0^t d\tau\ K(t-\tau)Z(\tau), \tag{8}$$

where $\dot{Z}(t)$ means the time derivative of $Z(t)$. The procedure for calculating the memory function $K(t)$ was as follows. From the computed values of $Z(t)$ [Eq. (5)], we obtained the time derivative, i.e., the left-hand side of Eq. (8). Then, starting from an initial approximation for 50 points of the memory function $K(t)$ uniformly distributed within the range $0-t_{\max}$, where $t_{\max}$ is the maximum time for which we computed $Z(t)$ (typically, 1–2 ps), we constructed an initial memory function for all times in which $Z(t)$ is defined using a cubic spline. The convolution, i.e., the right-hand side of Eq. (8), was then used to calculate an approximated time derivative, which was compared with the exact value previously computed to obtain the mean square deviation of the initial approximation for $K(t)$. The software package MERLIN [30] was then used to optimize the 50 values of the memory function $K(t)$ by minimizing such a mean square deviation.

The initial value of the memory function $K(t)$ gives the square of the Einstein frequency, ω_E, which can also be directly evaluated from the MD simulation data using the expression

$$\omega_E^2=\frac{\sum_{i=1}^{N}\langle F_i^2\rangle}{2m\langle E_{\rm kin}\rangle}, \tag{9}$$

where F_i is the total force exerted on atom i. Both methods for calculating ω_E gave results in very good agreement for all metals studied in this paper.

The time-dependent elements of the microscopic stress tensor are given by

$$J_{\alpha\beta}(t)=m\sum_{i=1}^{N} v_i^\alpha(t)v_i^\beta(t)+\sum_{i=1}^{N-1}\sum_{j=i+1}^{N} r_{ij}^\alpha(t)F_{ij}^\beta(t), \tag{10}$$

where v_i^α is the α component of the velocity of atom i, r_{ij}^α is the α component of the vector $\mathbf{r}_{ij}$ separating atoms i and j, and F_{ij}^β is the β component of the force exerted by atom i on atom j. By considering the off-diagonal elements of the stress tensor, we computed the stress autocorrelation function $\eta(t)$ as

$$\eta(t)=\frac{1}{3VkT}\sum_{\alpha\beta}\langle J_{\alpha\beta}(t)J_{\alpha\beta}(0)\rangle, \tag{11}$$

where the sum is to be made on the circular permutation of the indices $\alpha\beta$ (xy, xz, and yz). From the stress autocorrelation function, the shear viscosity was obtained using the Green-Kubo-like formula

$$\eta_s=\int_0^\infty dt\ \eta(t). \tag{12}$$

The shear viscosity was also computed using the Einstein-like equation

$$\eta_s=\frac{1}{2VkT}\lim_{t\to\infty}\frac{L_s^2(t)}{t}, \tag{13}$$

$L_s^2(t)$ being a ''mean square displacement,'' related to the off-diagonal elements of the stress tensor by

$$L_s^2(t)=\left\langle \left[\int_0^t d\tau\ J_{\alpha\beta}(\tau)\right]^2 \right\rangle, \tag{14}$$

where the angular brackets denote average both over a number of 7360 time origins and the nondiagonal indices of the stress tensor.

IV. THEORY

In the theoretical calculation of dynamic properties of a liquid, the static structure is required as an input. This has been obtained within the variational modified hypernetted chain (VMHNC) theory [31,32].

For the computation of the dynamic properties and the transport coefficient, we follow the theory proposed in Ref. [23], which enables, within certain approximations, the self-consistent determination of all the one-particle time correlation functions. This is briefly described below.

A. Self-diffusion

The key magnitude in the theoretical study of the one-particle dynamics of a liquid is the memory function of the velocity autocorrelation function, $K(t)$. This function can be split into two contributions [20,33],

$$K(t)=K_B(t)+K_{\mathrm{MC}}(t), \tag{15}$$

which represent two distinct dynamical regimes. The first term, $K_B(t)$, comprises all the fast decay channels and is supposed to represent the effects of a ''binary'' collision between the tagged particle and another one from the surrounding environment. The second term, i.e., the mode-coupling contribution $K_{\mathrm{MC}}(t)$, incorporates the effects of multiple collisions through the coupling with slowly decaying collective properties.

1. Binary contribution

At very short times the memory function is dominated by $K_B(t)$, and in fact the initial value $K(0)$ and the curvature at $t=0$, $\ddot{K}(0)$, are given by the corresponding values of K_B. The short time expansion of $K(t)$,

$$K(t)=K(0)\left[1-\left(\frac{t}{\tau_D}\right)^2+\cdots\right], \tag{16}$$

defines the initial decay time τ_D,

$$\tau_D=\left[\frac{|\ddot{K}(0)|}{2K(0)}\right]^{-1/2}. \tag{17}$$

Moreover, these quantities depend only on the static structure of the liquid. As stated above, the initial value of the memory function is given by the Einstein frequency squared, ω_E^2, which can be obtained from the pair potential and the radial distribution function,

$$K(0)=K_B(0)=\omega_E^2=\frac{\rho}{3m}\int d\mathbf{r}\; g(r)\nabla^2\phi(r). \tag{18}$$

The initial curvature, and therefore τ_D, is also determined by the static structure, but in this case there is a contribution arising from the three-body distribution function $g^{(3)}(\mathbf{r},\mathbf{r}')$,

$$\begin{aligned}\ddot{K}(0)&=\ddot{K}_B(0)\\&=-\frac{2\rho}{m^2}\int d\mathbf{r}\left\{\nabla_{\mathbf{r}}\left[\frac{z\phi'(r)}{r}\right]\right\}^2 g(r)\\&\quad-\left(\frac{\rho}{m}\right)^2\int d\mathbf{r}\int d\mathbf{r}'\nabla_{\mathbf{r}}\left[\frac{z\phi'(r)}{r}\right]\nabla_{\mathbf{r}'}\left[\frac{z'\phi'(r')}{r'}\right]\\&\quad\times[g^{(3)}(\mathbf{r},\mathbf{r}')-g(r)g(r')].\end{aligned} \tag{19}$$

The three-body contribution to τ_D is computed by using the simple superposition approximation for the three-body distribution function, i.e.,

$$g^{(3)}(\mathbf{r},\mathbf{r}')=g(r)g(r')g(|\mathbf{r}-\mathbf{r}'|). \tag{20}$$

Within this approximation, the second integral in Eq. (19) is conveniently evaluated in q space, as noted in Ref. [23] (see also Ref. [34]).

Finally, for $K_B(t)$ we use a simple semiphenomenological approximation that reproduces the correct short time expansion. There are of course many functions that fulfill this requirement. In the literature the most widely found are the hyperbolic secant squared (ThS) and the Gaussian (ThG) forms. Although both of them start in exactly the same way, their tails are different; in fact, the hyperbolic secant squared is somewhat wider than the Gaussian. In this paper we will consider both of them, namely,

$$K_B(t)=\omega_E^2\,\mathrm{sech}^2(t/\tau_D) \tag{21}$$

and

$$K_B(t)=\omega_E^2\,\exp[-(t/\tau_D)^2]. \tag{22}$$

Note that in this way the binary contribution to $K(t)$ is evaluated from the static structural functions only.

2. Mode-coupling component

In Eq. (15), $K_{\mathrm{MC}}(t)$ takes into account the coupling between the dynamics of the tagged particle and slowly decaying collective modes, which results in a long time tail in the memory function. This long time tail in $K(t)$ has been known to be essential in the correct description of the one-particle dynamic properties since the pioneering analysis of Levesque and Verlet [35]. A rigorous treatment of this term requires the use of kinetic and mode-coupling theories, and the actual details can be found, for instance, in Ref. [33]. In principle, several couplings should be considered (density-density, density-longitudinal currents, and density-transverse currents), but for systems near the melting point the most important contribution comes from the density-density coupling. This has been observed in calculations for liquid Rb [36], liquid Na [11], and liquid Pb [37] in thermodynamic states close to melting.

We therefore restrict to density-density coupling, which leads to the following expression for $K_{\mathrm{MC}}(t)$:

$$\begin{aligned}K_{\mathrm{MC}}(t)=\frac{\rho kT}{6\pi^2 m}\int_0^\infty dq\; q^4c^2(q)[&F_s(q,t)F(q,t)\\&-F_s^B(q,t)F^B(q,t)].\end{aligned} \tag{23}$$

Here $c(q)$ denotes the direct correlation function, and $F(q,t)$ and $F_s(q,t)$ are the intermediate scattering function and its self-part, whereas the superscripts B denote the corresponding ''binary'' parts.

In order to evaluate the integral of Eq. (23), we need to use some approximations for the intermediate scattering functions and their binary parts (see Ref. [23] for details). First, the binary part of the self-intermediate scattering function is taken as that of an ideal gas,

$$F_s^B(q,t)=F_0(q,t)\equiv\exp\left[-\frac{kT}{2m}q^2t^2\right]. \tag{24}$$

Second, we assume that the ratio between $F(q,t)$ and its binary part can be approximated by the ratio between their corresponding self-parts,

$$F^B(q,t)=\frac{F_s^B(q,t)}{F_s(q,t)}F(q,t). \tag{25}$$

For $F(q,t)$ we use the well known viscoelastic model with a relaxation time determined by Lovesey's scheme [38]. Note that within this approach $F(q,t)$ is also determined only by the static structure of the liquid. Finally, for $F_s(q,t)$ we use the Gaussian approximation [26]

$$F_s(q,t)=\exp[-\tfrac{1}{6}q^2\langle\Delta r^2(t)\rangle], \tag{26}$$

which gives correct results for small and large q, and also has the correct behavior at short times.

3. Self-consistent procedure

The binary part of the memory function $K_B(t)$ and the intermediate scattering function $F(q,t)$ are given in terms of the static structural properties only. The binary part of the self-intermediate scattering function is given by the ideal gas result, which depends only on the temperature of the system. On the other hand, $F_s(q,t)$, and through it $F^B(q,t)$, depend on the mean square displacement [Eqs. (26) and (25)]. This means that the mode-coupling contribution to the memory function, $K_{\rm MC}(t)$ [Eq. (23)], depends on $\langle\Delta r^2(t)\rangle$. But the mean square displacement can be obtained from the velocity autocorrelation function $Z(t)$ [Eq. (7)], which itself is determined by the memory function [Eq. (8)]. Therefore, we arrive at a self-consistency problem, displayed in Fig. 2. Starting from some estimate of $K_{\rm MC}(t)$, and using the known values of $K_B(t)$, we obtain $K(t)$ from Eq. (15). From this we compute $Z(t)$ through Eq. (8), and the mean square displacement [Eq. (7)]. The Gaussian approximation then determines $F_s(q,t)$. This is then used to obtain $F^B(q,t)$ which, together with the known values of $F(q,t)$ and $F_s^B(q,t)$, leads to a new estimate of $K_{\rm MC}(t)$ through Eq. (23). This loop is then iterated until self-consistency between input $K_{\rm MC}$ and output $K_{\rm MC}$ is achieved.

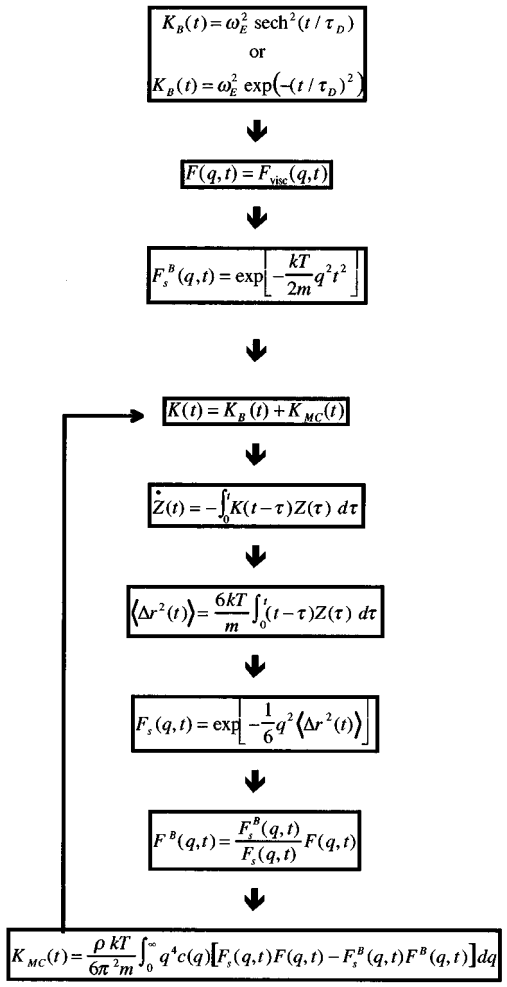

FIG. 2. Algorithm for the self-consistent determination of $K(t)$.

B. Shear viscosity

The microscopic stress tensor [Eq. (10)] has a kinetic term and a potential term. Therefore, the stress autocorrelation function $\eta(t)$ has three different components: a purely potential term, a purely kinetic term, and a cross term. Previous studies [23,39] have shown that in thermodynamic states near melting the last two contributions are rather small, and therefore the stress autocorrelation function is well approximated by its potential part only. In a similar way as the memory function of the velocity autocorrelation function, this purely potential contribution to $\eta(t)$ can be separated in two parts: a ''binary'' part and the mode-coupling contribution

$$\eta(t)=\eta_B(t)+\eta_{\rm MC}(t). \tag{27}$$

As we did in the case of self-diffusion, we will use the two different *Ansätze* for the binary component, namely, the ThS *Ansatz*,

$$\eta_B(t)=G_p\,\mathrm{sech}^2(t/\tau_\eta), \tag{28}$$

and the ThG one,

$$\eta_B(t)=G_p\exp[-(t/\tau_\eta)^2], \tag{29}$$

where G_p, the rigidity modulus, is the initial value of both $\eta(t)$ and $\eta_B(t)$, and τ_η is their common initial decay time. These two magnitudes can again be obtained from the static structure of the system only [23]. The superposition approximation for $g^{(3)}$ is also used in the evaluation of τ_η.

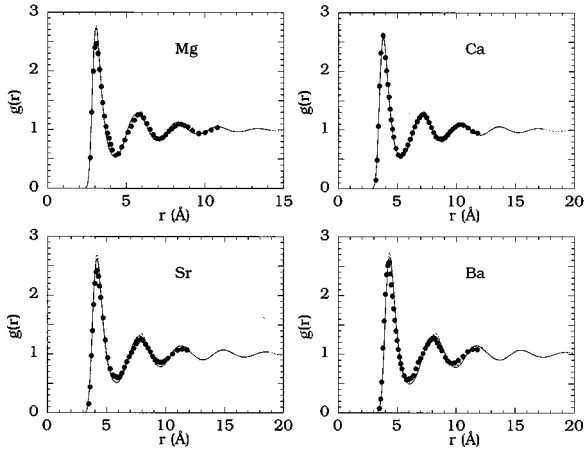

FIG. 3. Pair distribution function of the liquid alkaline earths. Solid line: MD simulations; dotted line: VMHNC calculations (Ref. [19]); full circles: Fourier transform of the experimental structure factor (Ref. [15]).

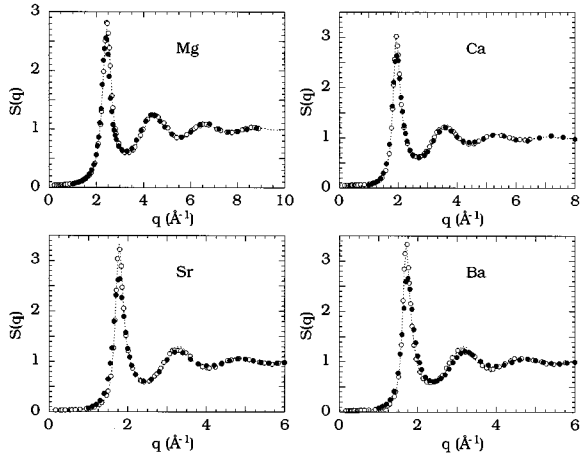

FIG. 4. Static structure factor of the liquid alkaline earths. Open circles: MD simulations; dotted line: VMHNC calculations (Ref. [19]); full circles: experiment (Ref. [15]).

The mode-coupling term, in the approximation of considering only density-density couplings, is given by

$$\eta_{\mathrm{MC}}(t)=\frac{kT}{60\pi^2}\int_0^\infty dq\ q^4\left[\frac{S'(q)}{S^2(q)}\right]^2\{F(q,t)^2-F^B(q,t)^2\}. \tag{30}$$

Within the approximations stated above for the intermediate scattering functions and their binary parts, we can evaluate this integral once we know the mean square displacement, for which we use the one obtained through the self-consistent procedure.

V. RESULTS

A. Static structure and thermodynamics

In a previous paper [19] the VMHNC theoretical results for the structure factor were compared with the experimental ones [15], and the theoretical $g(r)$ with that deduced from Fourier inversion of the experimental $S(q)$, and also for comparison with computer simulations carried out using a different interionic potential [18]. In this section we include in the discussion the MD results obtained from the NPA potential as calculated in this work.

In Fig. 3 we show the pair distribution functions $g(r)$ for the alkaline earths near their melting point. The agreement between the theoretical results and the simulation data is excellent, and only minor discrepancies exist regarding the height of the peaks, especially in the cases of Sr and Ba. For these systems the values obtained from the inversion of the experimental structure factor are somewhat closer to the simulation than to the theoretical results, in particular in the region around the second peak of $g(r)$.

The static structure factors are shown in Fig. 4, where the theoretical results are plotted together with Waseda's experimental data and the simulated $S(q)$, obtained using Eq. (2). The experimental structure factors closely follow the results obtained from both the VMHNC theory and the MD simulation, which are themselves almost coincident for the q values computed in the simulation. In particular, the height of the main peak of $S(q)$, which was overestimated by the theory for the heavy elements [19], is reproduced by the simulations, showing that this fact is to be ascribed to the pair potentials used and not to some failure of the liquid state theory. As explained in Ref. [19], it is expected that a proper inclusion of polarizability effects would lead to a lowering of this peak.

As we mentioned above, the computation of thermodynamic quantities of metals by computer simulations is complicated due to the density dependence of the effective pair potentials, and also to the presence of a structure-independent, but density-dependent, volume term, which appears in the formulas for the thermodynamic quantities (in particular, the energy and the pressure). All the contributions to the thermodynamic properties coming from these terms and from the explicit density dependence of the pair potential are ignored in computer simulations, and therefore direct comparison with experiment is not always possible.

One magnitude not affected by these problems is the specific heat at a constant volume, which we computed from Eq. (1). Unfortunately, we are not aware of experimental measurements of this particular property. Therefore we compared the simulation results for C_v with values calculated from the VMHNC theory. This comparison is shown in Table II,

TABLE II. Structure dependent energy per particle (in units of kT) and constant volume specific heat per particle (in units of k) for the liquid alkaline earths. The uncertainties of the MD results are given in parentheses.

	E_{str}/NkT		C_v/Nk	
	MD	Theory	MD	Theory
Mg	-2.202	-2.201	3.02	3.013
	(0.001)		(0.09)	
Ca	-6.602	-6.619	3.30	3.342
	(0.001)		(0.09)	
Sr	-7.355	-7.340	3.5	3.549
	(0.002)		(0.1)	
Ba	-10.220	-10.093	3.7	3.612
	(0.003)		(0.1)	

TABLE III. Initial decay time for $K(t)$, squared Einstein frequencies and diffusion coefficients for the liquid alkaline earths. The MD ω_E^2 results shown are those computed using Eq. (9). The uncertainties of the MD results are given in parentheses.

	τ_D (ps)	ω_E^2 (ps^{-2})		D (Å^2/ps)		
	Theory	MD	Theory	MD	ThS	ThG
Mg	0.038 65	1006.17 (0.03)	998.74	0.665 (0.005)	0.582	0.646
Ca	0.063 29	411.93 (0.02)	411.76	0.606 (0.006)	0.631	0.702
Sr	0.1037	165.09 (0.03)	165.78	0.321 (0.004)	0.391	0.435
Ba	0.1380	97.47 (0.02)	97.65	0.233 (0.004)	0.305	0.332

where we see a good agreement between both sets of results.

Even though the total energy, as explained above, cannot be obtained by computer simulations, the structure-dependent term can be straightforwardly computed and compared with theoretical predictions. This comparison is also shown in Table II, again observing a very good agreement between VMHNC data and MD results.

B. Time-dependent and transport properties

We applied the theoretical iterative scheme described above to compute the memory function of the velocity autocorrelation function, along with the velocity autocorrelation function, the mean square displacement, and the diffusion coefficients of the alkaline earths near their melting points. Moreover, we computed the stress autocorrelation function and the shear viscosity using the theoretical formalism considered above. These are compared with the ''exact'' MD results for the same interionic potentials, and, where appropriate, also with experimental data.

1. Self-diffusion

The values of the initial decay time of the memory function, τ_D, for the alkaline earths, together with their squared Einstein frequencies, are shown in Table III, where we can observe an excellent agreement between the theoretical ω_E^2 and the simulated ones. This is a consequence of the good description of $g(r)$ by the VMHNC theory. It is also observed that, as we go from Mg to Ba, the initial decay time increases, and the Einstein frequency decreases, due mostly to the increase in the mass of the atoms.

The total memory functions are plotted in Fig. 5, where we have included the MD memory function and the theoretical $K(t)$ according to the ThS and ThG *Ansätze* for its binary part. It is observed that the behavior of the memory function for short times is clearly dominated by the binary contribution. We observe that the correct decay of $K(t)$ is better reproduced by the ThG *Ansatz* in the case of Mg, by the ThS *Ansatz* in the case of Sr and Ba, and is in between both theoretical results in the case of Ca.

The binary and mode-coupling contributions are shown in Fig. 6 in reduced units ($t^*=t/\tau_D$ and $K^*=K/\omega_E^2$). We have included in the figure the total MD memory function, which is equal to the exact ''mode-coupling'' term when the binary

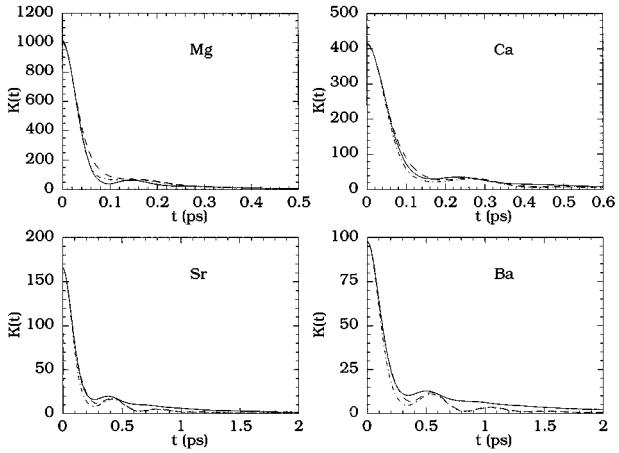

FIG. 5. Memory function of the velocity autocorrelation function. Solid line: MD simulations; dashed line: theoretical ThS calculations; dot-dashed line: theoretical ThG calculations.

contribution has decayed to zero, i.e., for $t^*>3.5$ approximately. The theoretical mode-coupling contribution is observed to change very little when we use either the ThS or the ThG *Ansätze*. It exhibits a typical behavior for all the systems. It shows a first peak at short times around $t^*=1.5$–2.3, where the binary constribution is still large, or at least significant, followed by a minimum and then a second peak around $t^*=4$. For times larger than this the binary part has already decayed to zero and $K(t)=K_{\mathrm{MC}}(t)$. Its behavior in this region is oscillatory around a slowly decaying tail. The same is also true for the MD memory function.

As we go from Mg to Ba we see the following trends. The first peak in K_{MC}^* keeps almost the same height, but moves to smaller values of t^*. On the other hand, the height of the second peak and the amplitude of the subsequent oscillations around the decaying tail increase as we move down the alkaline-earth series. When compared with the MD data, one can observe that the theoretical functions show, in general, too large an amplitude of the oscillations; these are shifted toward slightly larger values of t^*, and the amplitude of the

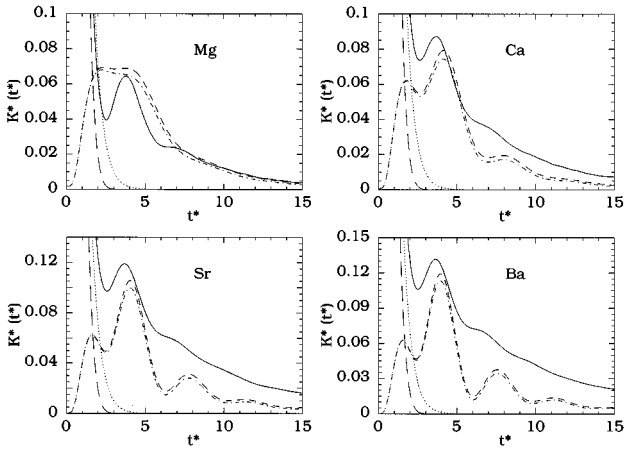

FIG. 6. Scaled mode-coupling component of the memory function. Solid line: total MD memory function; dashed line: theoretical ThS calculations; dot-dashed line: theoretical ThG calculations; dotted line: ThS binary contribution to $K(t)$; long dashed line: ThG binary contribution.

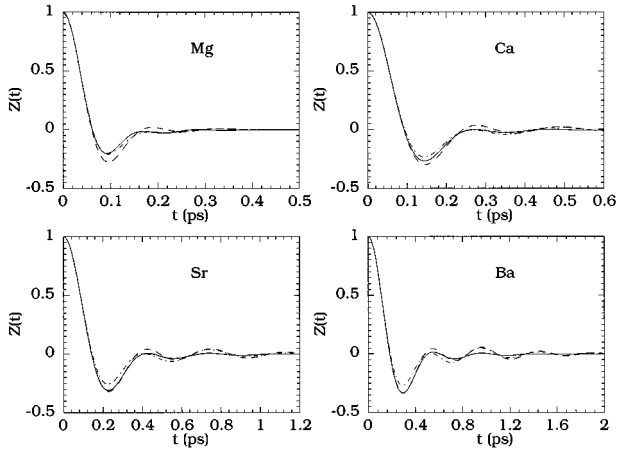

FIG. 7. Normalized velocity autocorrelation function. Solid line: MD simulations; dashed line: theoretical ThS calculations; dot-dashed line: theoretical ThG calculations.

decaying tail is too small, and slightly more so when using ThG. The case of Mg is special since in this case the long time behavior is just correct, but the intermediate time region is badly described by the theoretical K_{MC} since it is definitely too large when compared with the simulated $K(t)$. With respect to the binary terms, it is observed that in general the Gaussian form is somewhat too narrow, except in the case of Mg, where one can see that the hyperbolic secant squared is too wide, in fact wider than the total MD results.

In Fig. 7, we show the normalized velocity autocorrelation function for all the systems. The MD $Z(t)$ shows the backscattering minimum typical of high density systems at times around $t=2.2\tau_D$ followed by rather small oscillations around zero. The $Z(t)$ obtained from the theoretical memory functions show a similar behavior, with small deficiencies similar to those found for $K(t)$. It is observed that both theoretical approaches merge into one another for long times. As a consequence of the behavior of $K(t)$, we see that in general the oscillations at long times are somewhat overestimated. For shorter times, up to the second minimum of $Z(t)$, we see that, as was the case for $K(t)$, the ThS results are better for Sr and Ba, whereas in the case of Mg the ThG *Ansatz* gives better agreement with the simulations. For Ca, both results are rather similar and the simulation is in between.

The diffusion coefficients obtained from these $Z(t)$ are shown in Table III. Unfortunately, no experimental measurements of this property have been made, at least to our knowledge, and therefore we can only compare theoretical results with simulation ones. The diffusion coefficient can be obtained from the velocity autocorrelation function or from the mean square displacement. As we said before, both methods gave consistent results in the simulations and also in the theory. There is still another way of computing D, since its inverse is related to the time integral of the memory function $K(t)$, namely,

$$D^{-1}=\frac{m}{kT}\int_0^\infty dt\ K(t). \tag{31}$$

From this relation we can make an interpretation of the discrepancies found between the simulation results for D and the theoretical data.

Consider first the ThS results. Then it is observed that in the case of Mg the intermediate time values of the theoretical $K(t)$ are too large. This makes the integral too large, and therefore the theoretical diffusion coefficient is smaller than the simulated one. On the other hand, for Ca, Sr, and Ba the long time tail is too small when compared with simulation results, and therefore the integral is too small and the diffusion coefficients are larger than the simulated ones.

If we now focus on the ThG results we can see that, as commented upon before, the mode-coupling tail is somewhat smaller than the ThS one. Moreover, the binary part is also narrower. Both facts lead to decreasing the integral and therefore increasing the values of the diffusion coefficients. In the case of Mg, this leads to a much better agreement with simulation; however, for Ca, Sr, and Ba, where the ThS diffusion coefficient was already too large, its increase leads to a worsening of the results.

Some discussion is now in order so as to consider what are the possible reasons for these discrepancies between simulated and theoretical $K(t)$. There are several possibilities related to the different approximations made in the theory, namely (i) the neglect of the coupling integrals other than the density-density one; (ii) the Gaussian approximation [Eq. (26)] made for the self intermediate scattering function $F_s(q,t)$; and (iii) the viscoelastic approximation used for the intermediate scattering function $F(q,t)$.

(i) In the original theory [20,33] there are three other mode-coupling integrals related to the derivative of the intermediate scattering functions with respect to time and longitudinal and transverse currents. These three terms are supposed to be small for the density-temperature region we are exploring in this paper. However, the inclusion of these terms may lead to some improvement over the results obtained when they are neglected. We performed the actual calculations with these three extra terms included, and found no essential improvement. In fact, in all cases the decaying tail becomes slightly smaller, mainly due to the coupling with the derivative of $F(q,t)$, thus worsening the comparison with MD and slightly increasing the value of the diffusion coefficients. Moreover, in the case of Mg the intermediate time behavior is very similar when including the extra terms, so no improvement with respect to this problem is obtained either.

(ii) The Gaussian approximation fulfills a number of asymptotic limits (small q, large q, and small t), but it is still an approximation, and its accuracy has to be checked. This is not possible in this work since we have not calculated the ''exact'' MD q-dependent dynamic properties [$F_s(q,t)$ and $F(q,t)$]. However, in Ref. [23] it was shown that in the case of liquid Li near melting the deficiencies introduced by the Gaussian approximation in the self-dynamic structure factor $S_s(q,\omega)$ [which is the Fourier transform of $F_s(q,t)$] are rather small, and restricted to the frequency region close to $\omega=0$. This means that the Gaussian approximation is a rather good one, and therefore we expect that a more rigorous treatment of $F_s(q,t)$, although desirable, would not introduce large differences into the final results.

TABLE IV. Initial decay time for $\eta(t)$, and rigidity moduli and shear viscosities for the liquid alkaline earths. The uncertainties of the MD results are given in parentheses.

	τ_η (ps)	G_p (GPa)		η (GPa ps)			
	Theory	MD	Theory	MD	ThS	ThG	Expt.
Mg	0.05568	13.9 (0.2)	13.54	1.07 (0.08)	1.16	1.08	1.16 [a]
Ca	0.1004	8.2 (0.3)	8.20	1.20 (0.09)	1.29	1.20	1.20 [a]
Sr	0.1815	6.7 (0.3)	6.66	2.1 (0.1)	2.03	1.89	
Ba	0.2546	5.9 (0.2)	5.67	2.4 (0.2)	2.40	2.23	1.74 [a]

[a]From Ref. [17].

(iii) The viscoelastic approximation, with Lovesey's prescription for the relaxation time, is a very well known theory, and has been used for a discussion of the dynamic properties of a large number of systems, including recently binary alloys [40]. It is known to be a very good approximation in the vicinity of the first peak of the static structure factor, and it gives a rather accurate description of the dispersion relation, i.e., the position of the ω peak in the dynamic structure factor $S(q,\omega)$ as a function of q. However, the exact shape of $S(q,\omega)$ is not very well described for q values smaller than the first peak of $S(q)$, meaning also that the viscoelastic $F(q,t)$ may have significant discrepancies with the MD one in this q region. As we explained above, we cannot make a direct comparison in this case, since the MD $F(q,t)$ have not been computed, but we suggest that the use of the viscoelastic approximation is the main reason for the discrepancies found between the theoretical and MD memory functions.

MD calculations of $F_s(q,t)$ and $F(q,t)$ are now under progress, and they will be reported upon completion. Furthermore, within the theoretical framework of mode couplings, it is also possible to write down the intermediate scattering functions (strictly speaking, the second order memory function) as a sum of a binary term and a mode-coupling component. This approach is also under development, and will be reported in due course.

2. Shear viscosity

The initial values of the stress autocorrelation function and the initial decay times are displayed in Table IV. We see that the same trends as in the case of self-diffusion are observed, namely, τ_η increases and G_p decreases from Mg to Ba. Moverover, it is observed that the decay times for $\eta(t)$ are significantly larger than those associated with diffusion τ_D. The agreement between the rigidity moduli obtained theoretically and by MD simulations is very good.

In Fig. 8 we show the normalized $\eta(t)$ obtained from MD, and from the theory derived using the ThS *Ansatz*, together with the binary and mode-coupling terms of the latter. We will only comment on these theoretical results in order to keep the figures clear, but we will mention the ThG results later.

In contrast with self-diffusion, it is observed that even for very small times the binary term is too wide, especially in Sr and Ba. This means that the theory overestimates the values of τ_η. The reason for this lies on the approximation used for the three-body distribution function. The contribution coming from this term is comparatively larger in the case of τ_η (around 45%) than in the case of τ_D (around 10%), and therefore the errors in the superposition approximation are more noticeable in the former.

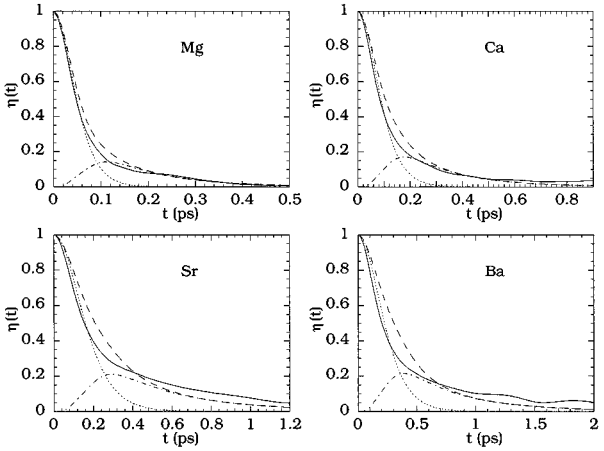

FIG. 8. Normalized stress autocorrelation function. The theoretical calculations correspond to the ThS *Ansatz*. Solid line: MD simulations; dashed line: theoretical calculations; dotted line: binary contribution; dash-dotted line: mode-coupling component.

The amplitude of the long time tail, on the other hand, is somewhat underestimated by the theory, especially for Sr and Ba. Despite these differences observed between the MD $\eta(t)$ and the theoretical one, it is observed in Table IV that the values for the shear viscosity obtained either from MD or from theory are in good agreement. Comparison with experimental data is also good for Mg and Ca, and reasonable for Ba.

The ThG results for the mode-coupling component are indistinguishable from those obtained through the ThS *Ansatz* in the scale of the graphs. On the other hand, the binary component is of course narrower. This therefore leads to smaller values of the shear visosities, which are also shown in Table IV.

VI. CONCLUSIONS

In this work we performed MD simulations of liquid alkaline-earth metals near their melting points using effective pair potentials which could be considered reliable in view of the agreement between previous theoretical calculations and experimental measurements of the static structure factor of these systems. We increased the confidence in the reliability of these potentials showing that the ''exact'' MD results for the structural properties do reproduce the behavior of the experimental structural data, and also of the only dynamic property we found in the literature, i.e., the shear viscosity. Moreover, the comparison of the thermodynamic properties and static structural data obtained by simulation with the theoretical predictions confirm the validity of the liquid state theory used.

Using these effective potentials, we also simulated a number of dynamic properties that, although not experimentally accessible, give physical insight so as to describe the dy-

namic behavior of the liquid, such as the velocity autocorrelation function, mean square displacement and stress autocorrelation function.

We have also used these simulations to check the validity of a recent self-consistent mode-coupling theory [23], making an analysis of the approximations involved in it. From this analysis we can obtain the following conclusions. (i) The superposition approximation for the three-body distribution function is accurate enough to describe the initial decay time of the physical processes associated with diffusion, but not for those associated with shear viscosity. In this case a more elaborate approximation, like the convolution approximation [41] or other recent approaches like that of Ref. [42], may be useful for a better description of the short time behavior of the stress autocorrelation function. (ii) We verified that both the hyperbolic secant squared and the Gaussian are valid functional forms for the binary part of the memory function of the velocity autocorrelation function and also of the stress autocorrelation function. The results of the application of the theory, within the other approximations made, slightly favors the hyperbolic secant squared, since it gives better global agreement with simulations than the Gaussian form, but this conclusion may change if better approximations are made. (iii) We verified that for the thermodynamic states considered in this paper, i.e., close to melting, the effects of couplings other than the density-density one are indeed small in the case of self diffusion, giving rise to a very small change in the theoretical results. We believe the same is also true for the stress autocorrelation function. (iv) We conclude that the theoretical efforts should therefore be directed to obtain a theory for the intermediate scattering functions more accurate than the simple viscoelastic model used here. Both MD simulations and mode-coupling calculations of $F(q,t)$ are currently being undertaken in order to validate this conclusion.

ACKNOWLEDGMENTS

We are grateful to D. J. González for useful discussions. Financial support provided by the DGI-CYT, Spain (Project No. PB95-0720-C02) and the Xunta de Galicia (Project No. XUGA20606B96) is also acknowledged.

[1] U. Balucani and M. Zoppi, *Dynamics of the Liquid State* (Clarendon, Oxford, 1994).

[2] P. Verkerk, P. H. K. de Jong, M. Arai, S. M. Bennington, W. S. Howells, and A. D. Taylor, Physica B **180-181**, 834 (1992); P. H. K. de Jong, P. Verkerk, S. Ahda, and L. A. de Graaf, in *Recent Developments in the Physics of Fluids*, edited by W. S. Howells and A. K. Soper (Hilger, Bristol, 1992); P. H. K. de Jong, P. Verkerk, and L. A. de Graaf, J. Non-Cryst. Solids **156**, 48 (1993); J. Phys.: Condens. Matter **6**, 8391 (1994).

[3] C. Morkel and W. Glaser, Phys. Rev. A **33**, 3383 (1986); C. Morkel, C. Gronemeyer, W. Glaser, and J. Bosse, Phys. Rev. Lett. **58**, 1873 (1987).

[4] C. Pilgrim, R. Winter, F. Hensel, C. Morkel, and W. Glaser, in *Recent Developments in the Physics of Fluids*, edited by W. S. Howells and A. K. Soper (Hilger, Bristol, 1992).

[5] C. Morkel and T. Bodensteiner, J. Phys.: Condens. Matter **2**, SA251 (1990); T. Bodensteiner, C. Morkel, W. Glaser, and B. Dorner, Phys. Rev. A **45**, 5709 (1992).

[6] D. L. Price, K. S. Singwi, and M. P. Tosi, Phys. Rev. B **2**, 2983 (1970).

[7] L. E. González, D. J. González, and K. Hoshino, J. Phys.: Condens. Matter **5**, 9261 (1993).

[8] L. E. González, D. J. González, M. Silbert, and J. A. Alonso, J. Phys.: Condens. Matter **5**, 4283 (1993).

[9] M. Canales, J. A. Padró, L. E. González, and A. Giro, J. Phys.: Condens. Matter **5**, 3095 (1993); M. Canales, L. E. González, and J. A. Padró, Phys. Rev. E **50**, 3656 (1994).

[10] U. Balucani, A. Torcini, and R. Vallauri, J. Non-Cryst. Solids **156**, 43 (1993); Phys. Rev. B **47**, 3011 (1993).

[11] F. Shimojo, K. Hoshino, and M. Watabe, J. Phys. Soc. Jpn. **63**, 1821 (1994); **63**, 141 (1994).

[12] A. Rahman, Phys. Rev. Lett. **32**, 52 (1974); Phys. Rev. A **9**, 1667 (1974).

[13] U. Balucani, R. Vallauri, and T. Gaskell, Phys. Rev. A **35**, 4263 (1987).

[14] S. Kambayashi and G. Kahl, Europhys. Lett. **18**, 421 (1992); Phys. Rev. A **46**, 3255 (1992); G. Kahl and S. Kambayashi, J. Phys.: Condens. Matter **6**, 10 897 (1994); G. Kahl, *ibid.* **6**, 10 923 (1994).

[15] Y. Waseda, *The Structure of Non-Crystalline Materials* (McGraw-Hill, New York, 1980).

[16] *Smithells Metals Reference Book*, edited by E. A. Brandes and G. B. Brook (Butterworth-Heinemann, Oxford, 1992).

[17] M. Shimoji and T. Itami, *Atomic Transport in Liquid Metals* (Trans Tech, Switzerland, 1986).

[18] W. Jank and J. Hafner, Phys. Rev. B **42**, 6926 (1990).

[19] L. E. González, A. Meyer, M. P. Iñiguez, D. J. González, and M. Silbert, Phys. Rev. E **47**, 4120 (1993).

[20] A. Sjölander, in *Amorphous and Liquid Materials*, edited by E. Lüscher, G. Fritsch, and G. Jacucci (Nijhoff, Dordrecht, 1987).

[21] U. Balucani, R. Vallauri, T. Gaskell, and S.F. Duffy, J. Phys.: Condens. Matter **2**, 5015 (1990).

[22] U. Balucani, A. Torcini, and R. Vallauri, Phys. Rev. A **46**, 2159 (1992).

[23] L. E. González, D. J. González, and M. Canales, Z. Phys. B **100**, 601 (1996).

[24] S. Nosé, Mol. Phys. **52**, 255 (1984).

[25] M. P. Allen and D. J. Tildesley, *Computer Simulation of Liquids* (Oxford University Press, Oxford, 1990).

[26] J. P. Boon and S. Yip, *Molecular Hydrodynamics* (McGraw-Hill, New York, 1980).

[27] J. P. Hansen and I. R. McDonald, *Theory of Simple Liquids* (Academic, London, 1986).

[28] J. M. Haile, *Molecular Dynamics Simulation* (Wiley, New York, 1992).

[29] C. Hoheisel, *Theoretical Treatment of Liquids and Liquid Mixtures* (Elsevier, Amsterdam, 1993).

[30] G. A. Evangelakis, J. P. Rizos, I. E. Lagaris, and I. N. Demetropoulos, Comput. Phys. Commun. **46**, 401 (1987).

[31] Y. Rosenfeld, J. Stat. Phys. **42**, 347 (1986).

[32] L. E. González, D. J. González, and M. Silbert, Phys. Rev. A **45**, 3803 (1992).

[33] L. Sjögren and A. Sjölander, J. Phys. C **12**, 4369 (1979).
[34] Note that in Eq. (10) of Ref. [23] the plus sign after $j_0(kr)$ should be substituted by a minus sign.
[35] D. Levesque and L. Verlet, Phys. Rev. A **2**, 2514 (1970).
[36] L. Sjögren, J. Phys. C **13**, 705 (1980).
[37] W. Gudowski, M. Dzugutov, and K. E. Larsson, Phys. Rev. E **47**, 1693 (1993).
[38] J. R. D. Copley and S. W. Lovesey, Rep. Prog. Phys. **38**, 461 (1975).
[39] U. Balucani, R. Vallauri, and T. Gaskell, Phys. Rev. A **37**, 3386 (1988).
[40] Ya. Chushak, T. Bryk, A. Baumketner, G. Kahl, and J. Hafner, Phys. Chem. Liq. **32**, 87 (1996).
[41] H. W. Jackson and E. Feenberg, Rev. Mod. Phys. **34**, 686 (1962); S. Ichimaru, Phys. Rev. A **2**, 494 (1970).
[42] J. L. Barrat, J. P. Hansen, and G. Pastore, Mol. Phys. **63**, 747 (1988).